Mesospheric observations with the EISCAT UHF radar during polar cap absorption events : 1. Electron densities and negative ions

P. N. COLLIS (1), and M. T. RIETVELD (2)

(1) *EISCAT Scientific Association, Box* 812, *S*-981 28 *Kiruna, Sweden*
(2) *EISCAT Scientific Association, Ramfjordmoen, N*-9027 *Ramfjordbotn, Norway*

Received April 24, 1990 ; revised July 3, 1990 ; accepted July 26, 1990.

ABSTRACT. Observations of mesospheric electron density were obtained by the EISCAT UHF radar during several polar cap absorption events (PCA's) in 1989. Both the latitudinal extent and the detailed vertical distribution of the excess ionisation were determined. Continuous observations over more than two days during one event allowed an investigation of the variations in electron density during four twilight intervals. It is shown that at sunrise, at heights above 70 km, electrons are released by ultraviolet photodetachment of a high-affinity negative ion, which may be NO_3^-. Below 66 km altitude, the increase of electron density is delayed by about 30 min, indicating that the time taken for neutral oxygen species to build up is a controlling factor in producing the free electrons at these heights. Both these processes are operative between 66 and 70 km altitude. Nighttime profiles of the ratio of negative ion number density to electron number density are deduced, and empirical relationships of electron concentration at heights between 60 and 70 km are determined as a function of simultaneously observed proton flux.

Annales Geophysicae, 1990, **8,** (12), 809-824

1. INTRODUCTION

Polar cap absorption (PCA) events are an ionospheric signature of the precipitation of energetic protons into the earth's atmosphere. The protons penetrate deep into the mesosphere causing much-enhanced *D*-region electron densities. The accompanying absorption of radio waves causes severe disruptions to HF and VHF radio communications in the polar regions where the particles are deposited, hence the term PCA (Bailey, 1964). Routine monitoring of such radio absorption has been possible since the late 1950's, when the riometer technique was introduced (Little and Leinbach, 1959). This instrument measures the amount of cosmic radio noise absorbed by the ionosphere at operating frequencies of about 30 MHz. Speculations that the particles causing PCA's were protons of solar origin were already aired before they could be detected by *in situ* experiments (Reid and Collins, 1959). Modern instruments carried on geostationary satellites are now able to provide continuous measurements of the flux and energy spectra of these particles.

The emission of protons from an active flare region on the sun is termed a solar proton event (SPE). The protons arrive at the earth between one and several hours after the flare, the delay depending mainly upon the heliographic longitude of the flare (Svestka, 1976). On reaching the magnetosphere, the protons are guided by the geomagnetic field and are preferentially deposited in the polar regions. Very high energies are needed for the particles to reach latitudes equatorward of the auroral zone (Reid, 1970) and the boundary of the PCA region is typically between 60 and 65° geomagnetic latitude. Durations of PCA's vary from a few hours to many days.

Ionisation in the lower *D*-region (50 to 70 km) during PCA's is caused mainly by protons with energies of the order of 10, or a few 10's MeV. Particles of greater energy can penetrate to the stratosphere, while a 500 MeV proton will reach tropopause levels. Such energetic events can be detected by ground-based neutron monitors, causing a so-called ground level effect (GLE). Observations of the ionospheric effects of SPE's, the realisation that the cause was indeed solar ejection of energetic protons, and the initiation of the study of *D*-region aeronomy all started with the very intense event of 23 February, 1956 (Bailey, 1959, and references therein). Much of the subsequent information on *D*-region characteristics during PCA events was gained from riometer measurements, particularly the day/night differences in absorption and twilight asymmetries (e.g. Eriksen *et al.*, 1960 ; Reid, 1961 ; Gillmor, 1963 ; Chivers and Hargreaves, 1965). The advantage of the riometer technique is its cheapness and simplicity of operation, but a drawback is

that the observations represent an integration over all heights where absorption is produced. Rocket experiments can give the missing height-dependent information, as well as more detailed aeronomical measurements (e.g. for negative ions, Narcisi *et al.*, 1971; Arnold *et al.*, 1982; Viggiano *et al.*, 1982). However, their duration is very limited in comparison to that of a typical PCA and multi-payload campaigns are necessary to cover all phases of an event (Ulwick, 1971). Continuous ionospheric measurements, including altitude variations, are possible with the incoherent scatter radar technique. In its simplest form, this method yields electron density as a function of height by measuring the amount of power returned by the ionosphere from a transmitted pulse (the power-profile technique). More complex processing can be used to determine the frequency spectrum of the scattered signal, which contains more information than the power alone (eg. Collis and Röttger, 1990).

The occurrence frequency of SPE's is a strong function of the 11-year solar cycle. Events are very rare for the 2 to 3 years near solar minimum, but about one per month, on average, can be expected near solar maximum. More strictly, the frequency and intensity of these events are found to be greatest about 1 year before and 2-3 years after the time of maximum sunspot number (Hakura, 1974). The present solar cycle (cycle 22, which started in September 1986) has so far matched the development of the previous most intense cycle (19) in terms of sunspot number and 10.7 cm radio flux (Solar Geophysical Data, 1989). The year 1989, which is about 1 year before the expected solar maximum, produced a much larger number of SPE's than have occurred in recent years, giving good opportunities for observations during PCA conditions.

The present paper discusses measurements by the EISCAT incoherent scatter radar from mesospheric heights during PCA events in 1989. Earlier observations from the Chatanika incoherent scatter radar during the strong SPE's of August 1972 were reported by Reagan and Watt (1976). One result was the determination of effective recombination coefficients in the *D*-region by combining electron densities measured by the radar with ionisation rates calculated from proton and alpha particle fluxes observed by satellite. The Chatanika measurements were obtained with a 67 μs pulse (10 km resolution) and 10-min averaged results were presented. A similar approach was adopted by Hargreaves *et al.* (1987) in the only other report to date of EISCAT observations during a PCA, which occurred on 16 February 1984. Improvements in technique allowed a resolution of 600 m in range to be used in that experiment, though further smoothing over 3 km was used, together with 10-min averaging in time.

EISCAT observations were obtained during seven of the eight most intense SPE's of 1989 (in terms of maximum particle flux). The present series of experiments included several new characteristics in comparison with earlier radar measurements during PCA conditions. By the use of a number of different transmitted pulse-code schemes and antenna scanning patterns from event to event, the available data include latitude scans, different ranges of altitude coverage and resolution (better than 1 km in some cases) and results from power profile, multipulse and pulse-to-pulse correlation measurements in the mesosphere. The latter technique, which allowed spectral measurements down to 50 km altitude in one case, has not previously been used during PCA conditions. A companion paper (Rietveld and Collis, 1990) concentrates on the results of the spectral measurements; in the present paper the emphasis is placed on observations of electron concentration.

2. THE SOLAR PROTON EVENTS OF 1989

Magnitudes of solar proton events are commonly quoted as the integral flux of particles exceeding 10 MeV, in units of $(cm^2\ s\ sr)^{-1}$, termed here proton flux units (pfu). For energetic events, the flux exceeding 100 MeV is a further measure. No effect is detectable by riometer for events less than 10 pfu (> 10 MeV) while only a small effect (< 1.5 dB) is expected for fluxes below 100 pfu (Smart and Shea, 1971). Table 1 lists those events from 1989 which exceeded 100 pfu, together with available information on radio-wave absorption measured by riometer.

Table 1

Solar proton (SPE) *and polar cap absorption* (PCA) *events during* 1989. *Particle flux is integral proton flux exceeding* 10 MeV *in units of* $(cm^2\ s\ sr)^{-1}$ *and* dB *is the maximum radio absorption measured by a* 30 MHz *riometer at Thule* ($L = 250$). *Only events exceeding* 100 pfu *are included. Times are given as day/hour* (UT). *Data originally published in Solar Geophysical Data* (1989). *The quoted proton fluxes may be overestimated by up to a factor of two (see text). Note that absorption values followed by an asterisk* (*) *are measured at* 51.4 MHz *from Sodankylä* ($L = 5.1$) *(Courtesy of Sodankylä Geophysical Observatory).*

SPE				PCA			
Start	End	Maximum		Start	End	Maximum	
		time	flux			time	dB
Mar 08/1730	14/1135	13/0745	3000	09/1700	14/1700	13/0800	6
Mar 17/1855	20/1720	18/0920	2000	17/2100	20/0600	18/1430	2.3*
Apr 11/1435	15/2025	12/0125	450	11/1900	14/1415	12/0101	5
May 06/0235	08/0945	06/1045	110	unclear	unclear	06/1200	1.8*
Aug 12/1600	28/0120	13/0710	9200	12/1800	20/1845	13/	30
Sep 29/1205	04/0145	30/0210	4800	29/1158	03/1815	29/2100	16
Oct 19/1305	30/1135	20/1600	73000	19/1315	29/1400	20/1400	8*
Nov 27/2000	29/1555	28/1105	380	unclear	unclear	28/1212	0.5*
Nov 30/1345	03/1800	01/1340	7300	30/1825	02/1800	01/1730	7

Two comments need to be added concerning the information in Table 1. First, the estimates of proton flux may be too large by up to a factor of two, depending on the hardness of the spectrum. This arose because of contamination of the lower energy channels by higher energy particles. A new estimate of the peak flux (> 10 MeV) for 20 October is now 40000 rather than the 73000 pfu initially quoted (Zwickl and Kunches, 1989). When quantitative use is made of the fluxes from the October event later in this paper, the values originally published in Solar Geophysical Data (1989) have been scaled down by a factor 0.55. The second point to note is that available values of radio absorption from Thule have been supplemented by data from Sodankylä, Finland ($L = 5.1$) to provide a complete list. Interference is currently a serious daytime problem for riometers operating at frequencies near 30 MHz in Scandinavia so we have taken absorption values from the 51.4 MHz riometer at Sodankylä. The equivalent absorption at 30 MHz can be obtained by multiplying the quoted values by 2.9 (according to the square of the frequency).

3. EISCAT OPERATIONS DURING THE SPE's OF 1989

Periods of availability of EISCAT data during PCA conditions in 1989 are listed in Table 2. Descriptions of the EISCAT facility have been given by Folkestad *et al.* (1983) and Baron (1984). The facility is situated in northern Scandinavia with transmitters located at Tromsö, Norway (69.6° N, 19.2° E, $L = 6.2$). Although tristatic data are available for some of the operations mentioned here (allowing estimates of vector electric fields), we will consider only monostatic measurements from Tromsö. Moreover, no data are available from the VHF radar during PCA conditions in 1989 — all the observations reported here were made with the UHF (933 MHz) system. In some cases, the radar was already in scheduled operation when the SPE occurred. For other cases, experiments were started when it became apparent that an event was underway.

The experiment modes fall into four classes with different measurement schemes for the mesosphere. Three of these modes (CP-1, CP-2 and CP-3) are general purpose, covering the *E*- and *F*-regions as well as the *D*-region, while the fourth (GEN-11) is designed specifically for mesospheric heights. These four schemes are now briefly described.

CP-3 is a wide-latitude scanning experiment employing 30-min scans from north to south with 17 individual antenna positions. The part of the experiment of interest here is the power profile with a resolution of several km in altitude and lowest sampled altitudes between 60 and 80 km, both dependent on antenna position. The latitudinal coverage of the scan at 90 km altitude is 4.5° (about 500 km). More details of this experiment scheme are given by Collis and Häggström (1988).

The CP-1 pulse scheme is identical to the one used in CP-2 and the two will be considered together here. (The differences between these two are in the antenna pointing : CP-2 scans through four positions in 6 min but the CP-1 transmitting antenna remains stationary.) Power profile measurements start at a range of 68 km. The lowest antenna position in CP-2 is at an elevation of 60°, resulting in a lowest altitude of 59 km for the power profile. The operations of the CP-1 scheme on 30 November and 1 December also used an elevation of 60°.

The GEN-11 scheme (Turunen, 1986) is quite different from the former three having been specially designed for mesospheric heights, utilising the pulse-to-pulse correlation technique. This scheme provides spectral measurements (as well as power) from 70 to 112 km range at 1.05 km intervals. During some of the PCA operations the antenna was tilted down to an elevation of 45°, which puts the first range-gate at a height of 50 km. However, the first five gates are seriously affected by self-clutter and in practice the sixth gate is the first usable one, at a height of 54 km for 45° elevation.

Table 2

EISCAT operations during PCA's in 1989. *Details of the experiment modes are given in the text.* NA *means mesospheric spectral measurements not available from experiment* CP-3. *Times are listed as day/hour* (UT).

Start	End	Mode	Lowest altitude (km) for power	spectra
Mar 10/0845	10/1700	GEN-11	70	70
Apr 10/1300	13/0700	CP-3	60	NA
Aug 12/2000	13/0400	GEN-11	66	66
Aug 13/2030	14/0500	GEN-11	66	66
Aug 14/2000	15/0200	GEN-11	66	66
Oct 02/0930	02/1050	GEN-11	70	70
Oct 20/0950	20/1230	GEN-11	50	50
Oct 23/1200	23/1755	GEN-11	54	54
Oct 23/1800	25/1430	CP-2	59	80
Nov 27/1000	29/1600	CP-3	60	NA
Nov 30/1725	30/2300	CP-1	58	80
Dec 01/0915	01/1126	GEN-11	57	57
Dec 01/1800	01/2200	CP-1	58	80

4. RESULTS

Wide scanning experiments

Both the April and November operations of CP-3 were regular scheduled experiments (Table 2), though the April one was timed specifically to coincide with an anticipated 27-day recurrence of the severe magnetic storm in March. The SPE's during the April and November CP-3 experiments were the least intense of the ones reported here. Neither of these events registered enhanced fluxes above 100 MeV. In CP-3, only four of the 17 antenna positions provide power profile measurements from altitudes below 68 km, hence latitudinal distributions of electron density below about 70 km altitude are not well defined. The lowest altitude common to all antenna positions is 80 km, but at this height energetic electrons can also be an important source of ionisation.

Durations of typical PCA's are long compared with the 30-min scan time in CP-3, and since the proton precipitation is spatially uniform, the temporal variations of electron density down to 60 km can be examined by using measurements from one antenna position which covers the lowest altitudes. Figure 1 shows the results from heights close to 65, 70, 75 and 80 km from the antenna position at elevation 42° to the south for the whole of the 10-13 April experiment, together with the proton fluxes. Several periods of enhanced density can be noticed: the largest values occurred between 00 and 04 UT on 12 April. The slow variations of electron density over periods of hours, together with the correlation of similar features at all heights, strongly suggest that energetic protons were the source of the increased densities. Some of the finer time structure at 80 km is likely to be due to electron precipitation, however. The interval of largest densities coincided with that of the most intense proton fluxes measured at geostationary orbit. Apart from this similarity, however, there was no other obvious correspondence between the temporal variations of *D*-region electron density and proton flux. Neither was there any clear day/night modulation of electron density. Note also that small density enhancements at 65 km were already present early in the experiment before the proton fluxes reached event level (> 10 pfu above 10 MeV) at 1435 UT on 11 April. Figure 1 shows that the > 10 MeV fluxes started to increase above background level on the afternoon of 10 April.

Latitudinal distributions of electron densities measured by EISCAT during the 10-13 April CP-3 experiment are shown in Figure 2. As a compromise between covering the widest possible range of latitudes and excluding the effects of electron precipitation, these data are from a height of 80 km. The shaded regions in Figure 2 indicate where very uniform electron densities with almost no irregular structure appeared (cf. Fig. 1). We infer that these regions are where the protons were deposited. EISCAT was apparently equatorward of the proton precipitation on the dayside but entered it on the nightside, providing scans through the edge of this region for most of 12 April and the early hours of 13 April. An example of the observations from a single scan through the edge of the proton precipitation region in the early morning of 12 April is shown in Figure 3. Densities were largest at the poleward edge of the scan where a layer of peak density 5×10^{10} m^{-3} at 90 km was present. Further equatorward, the layer was absent; instead, the densities

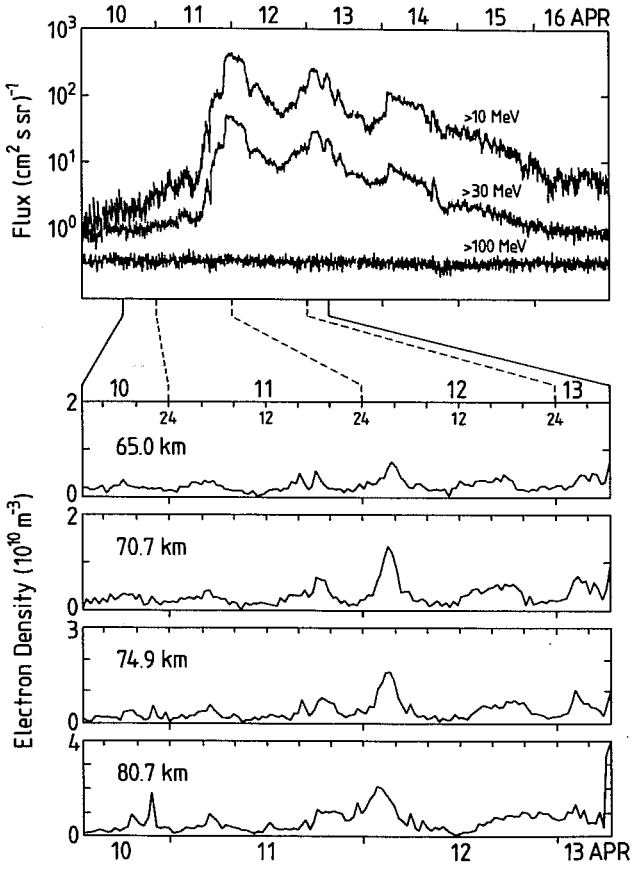

Figure 1

Lower panels: time series of electron densities from four D-region altitudes, measured by the EISCAT radar between 13 UT *on 10 April and* 07 UT *on* 13 *April,* 1989. *These data are from the scanning* CP-3 *experiment and represent* 90-s *averages taken every* 30 min *from the same antenna position directed at elevation* 42° *to the south.*

Upper panel: integral proton fluxes above three threshold energies measured onboard the geostationary satellite GOES-7 *during the* SPE *event in April* 1989 *(data courtesy of* NOAA*).*

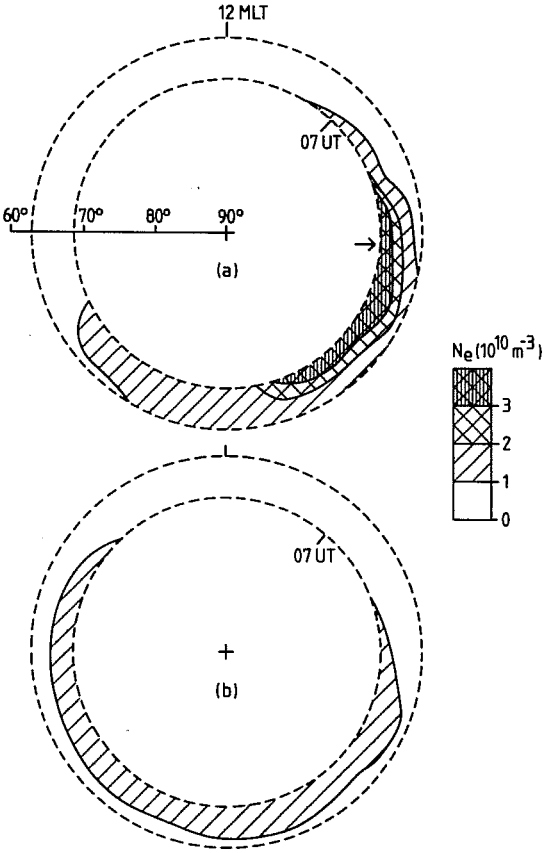

Figure 2

24-h *latitude-time distributions of electron density at* 80 km *altitude measured by EISCAT experiment* CP-3, 11-13 *April,* 1989. *The upper panel* (a) *starts at* 7 UT *on* 11 *April and the lower panel* (b) *at* 7 UT *on* 12 *April. Four levels of electron density are shown, according to the key. The arrow in the upper panel indicates the time of the scan in Figure* 3. *The coordinate system is geomagnetic latitude and magnetic local time* (MLT).

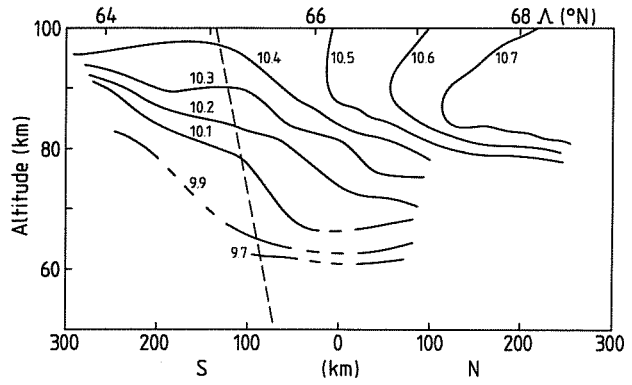

Figure 3

Latitude-altitude distribution of D-region electron density measured by EISCAT between 0330 *and* 0357 UT *on* 12 *April,* 1989, *when the earth's rotation was carrying the radar out of the region of proton precipitation. Broken lines indicate extrapolated contours. The straight line marks the position corresponding to the measurements in Figure* 4. *Distances are marked as* km *north* (N) *and south* (S) *of the transmitter site. Densities* (N_e) *are expressed as* $\log_{10}(N_e)$ m^{-3}.

decreased monotonically with decreasing altitude below 100 km. The time development of the density profiles through this phase of the event is illustrated in Figure 4, which shows successive profiles as measured in a single antenna position, i.e. every 30 min. For the period shown, between 0147 and 0517 UT on 12 April, the densities decreased with time for altitudes above 80 km and the layer peak originally at 90 km altitude eventually diminished to leave a profile of monotonically increasing densities between 60 and 100 km altitude. In contrast, at heights below 80 km an increase in density occurred over the first 60 to 91 min of the period shown, followed by a gradual decrease.

Without displaying the results of the November CP-3 experiment in detail, we can report that many features were similar to the April event. The magnitudes of the two events in terms of proton flux were almost the same and the maximum *D*-region densities and profile shapes were comparable with those in Figure 4.

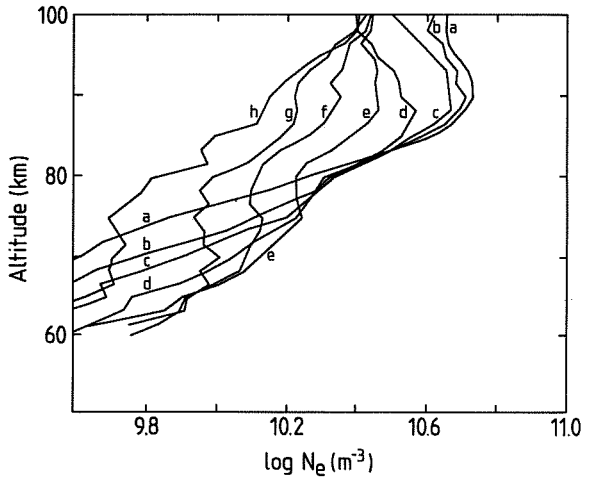

Figure 4

Time variation of electron density from a single antenna position in experiment CP-3, 12 *April,* 1989. *The results are* 90-s *averages taken every* 30 min *at antenna elevation* 53° *to the south, from* 0147 UT (a) to 0517 UT (h).

Temporal variations of the proton fluxes during the November event were simpler than those for the April one ; the former showed a gradual increase and decrease with a well-defined maximum. This simple behaviour was also seen in the EISCAT electron density measurements from 65 and 70 km altitude, but at 75 and 80 km the temporal variations were more complex than those in Figure 1, implying that energetic electrons were more prevalent in the November event.

Low altitude experiments with good height resolution

This category of observations comprises those termed GEN-11 in Table 2. Measurements were obtained with GEN-11 during the first major SPE of the year, on 10 March, between 0845 and 1700 UT. This was in the declining phase of the first maximum of proton flux ; values fell from about 200 to 70 pfu (> 10 MeV) during the EISCAT operation. As well as the fluxes being relatively low during this period, the energy spectra of the protons were very soft, with few particles more energetic than 30 MeV (Solar Geophysical Data, 1989). Vertical antenna pointing was used for the EISCAT measurements in this interval, giving an effective lowest altitude of only 75 km. Experience of operating this program under PCA conditions was gained in this run, but since better coverage at lower altitudes was obtained in other operations later in the year we do not discuss the March observations further here.

The EISCAT operations during the PCA event in August were fortuitous since they were obtained during a campaign of observations aimed at studying polar mesosphere summer echoes (Röttger *et al.*, 1988), hence the experiment mode was also well suited for PCA conditions. Detailed results from this event will be presented elsewhere (Turunen *et al.*, 1990).

Further operations of the GEN-11 experiment in October and December were initiated when it was realised that strong PCA's were in progress. The SPE which commenced on 29 September was particularly energetic during its early stages, producing the strongest GLE in 30 years (neutrons 500 % above background level, measured at Thule, Greenland). However, it was not possible, for operational reasons, to start observations with the EISCAT radar until the morning of 2 October, by which time the intensity of the SPE had diminished to only several 10's pfu (> 10 MeV). Electron densities measured by the radar were only 1×10^{10} m^{-3} at 87 km altitude and decreased rapidly at lower heights, with values much less than even the soft event in March. These measurements showed the weakest *D*-region of all the events discussed in this paper and will not be considered further in this study.

By far the most intense SPE of the year, in terms of total fluence, occurred later in October. EISCAT observations with the GEN-11 mode were obtained during the morning of 20 October, following the onset of the SPE, and again on 23 October when proton fluxes were still large. Figure 5 shows the proton fluxes measured at geostationary orbit for this event.

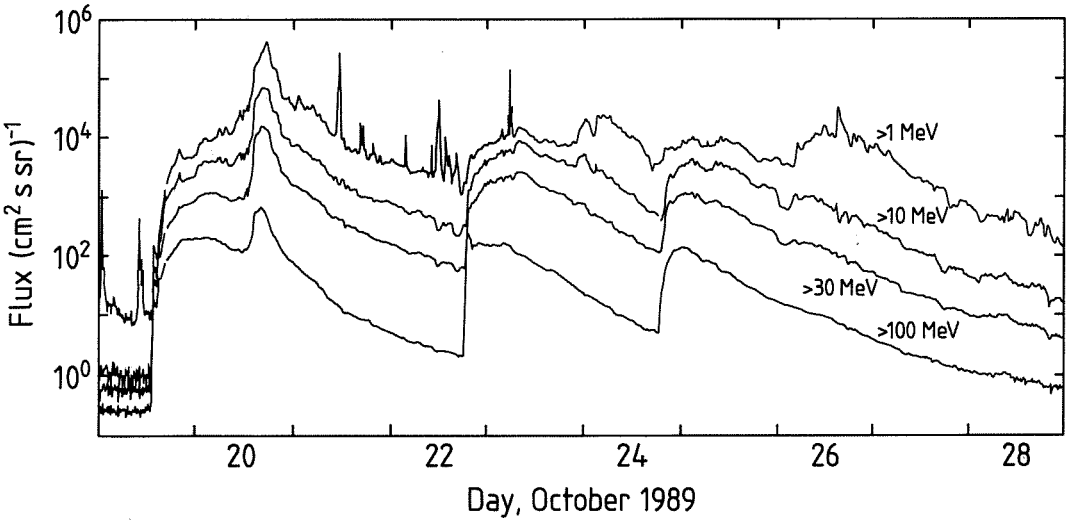

Figure 5
Integral proton fluxes for the interval 19-28 *October,* 1989 *(data courtesy of NOAA). Values for the lower energies may be overestimated by up to a factor of two (see text).*

The sharp onset at 1305 UT on 19 October was followed by a further burst on the afternoon of 20 October, producing the maximum fluxes of the event. Two further onsets occurred late on 22 October and late on 24 October. All these increases were accompanied by GLE's, with increases over background levels by 45, 25 and 90 %, respectively.

As soon as the radar observations began on 20 October, it was seen that strong signals were detected in all signal gates down to the lowest measured, at 70 km altitude. In order to obtain measurements from lower altitudes, the antenna, which was initially pointing vertically, was lowered in several steps to an elevation of 45° to the north. This resulted in the first useful signal gate appearing at 54 km altitude, which just included the bottom of the main *D*-region ionisation. Confirmation of the shape of the density profile at its lower edge was obtained by tilting the antenna to an elevation of 40° for 5 min, allowing coverage down to 49 km altitude. Figure 6 shows one of these profiles with results down to 50 km, together with another from 75 min earlier when the antenna was at a larger elevation (covering higher altitudes). The derived densities agree very closely for the overlapping altitudes. In fact, the observed densities were very uniform with time throughout this 150 min operation near local noon. Changes in solar zenith angle (χ) were small; from $\chi = 80°$ at the start of the experiment to 83° at the end.

Following the operation ending at 1230 UT on 20 October, EISCAT observations resumed with the GEN-11 scheme on 23 October, when proton fluxes were still comparable with those of 20 October. Examples of profiles from 23 October, from intervals when the solar zenith angle was about the same as on 20 October, are shown in Figure 7. The results in Figures 6 and 7, which are separated by three days,

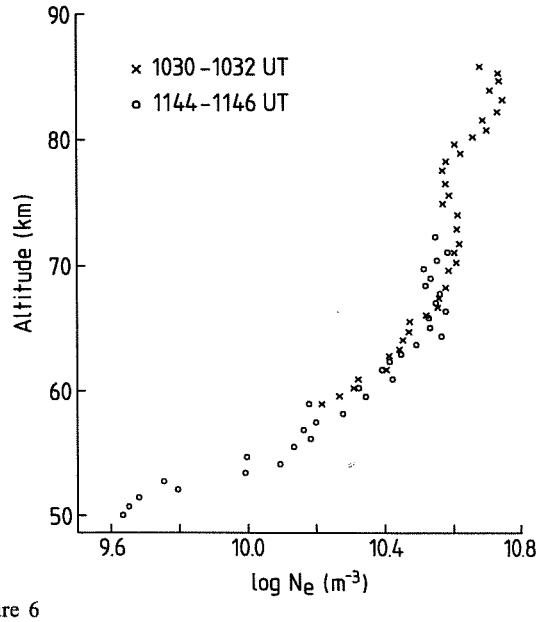

Figure 6
Two profiles of electron density from different antenna elevation angles during the operation of GEN-11 *on* 20 *October,* 1989.

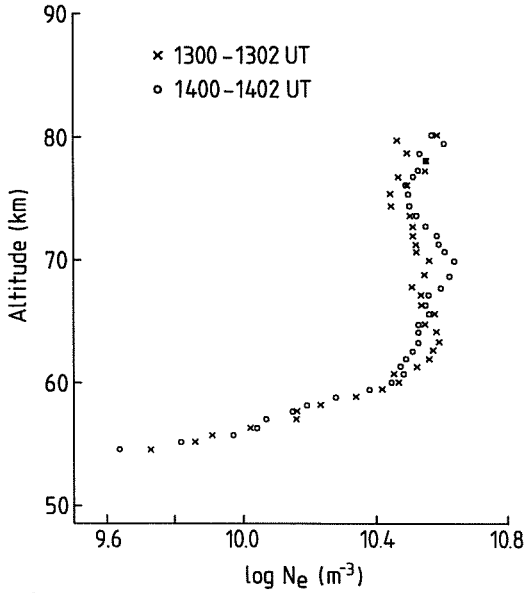

Figure 7
Two profiles of electron density from the GEN-11 *operation on* 23 *October,* 1989.

are very similar over most of the heights covered by the experiment, the main difference being that the densities fall away more rapidly below 58 km on 23 October. This observation is consistent with the slightly weaker energetic fluxes on 23 October (Fig. 5).

Measurements continued through the sunset period on 23 October. Figure 8*a* shows the observed electron density profiles in contour form, together with the solar zenith angle. Continuous measurements of power could be obtained throughout the experiment, but spectral signals were lost from progressively higher altitudes as the solar zenith angle increased, the signals disappearing at 90.2, 92.5, 94.5 and 98.2° at altitudes of 55, 60, 65 and 70 km respectively. Figure 8*b* shows examples of time series of electron density from selected altitudes, from which an impression of the noise level of the results can be gained ; the statistical uncertainty varies with signal strength but is typically better than 10 %. The broken line indicates the times of initial departure of electron density from steady daytime values. These move progressively upwards in altitude as the solar zenith angle gets larger. This solar zenith angle dependence will be discussed later.

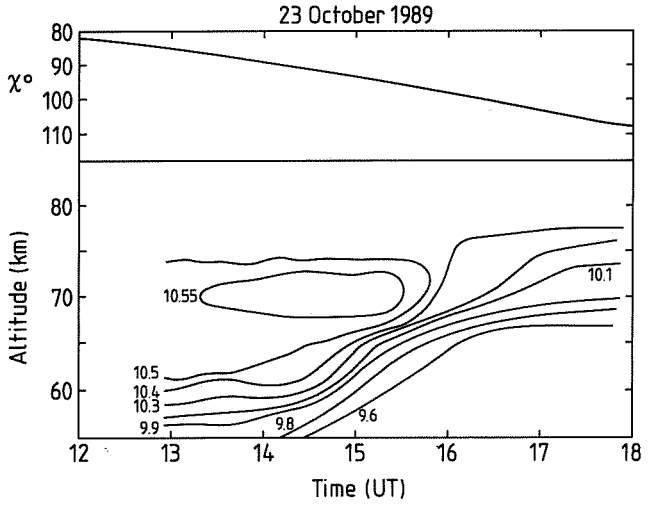

Figure 8*a*

Upper panel : solar zenith angle (χ) *for* 12 *to* 18 UT, 23 *October,* 1989.

Lower panel : contour representation of profiles of electron density from the GEN-11 *operation on* 23 *October,* 1989, *covering sunset. Densities* (N_e) *are expressed as* $\log_{10}$ (N_e) m^{-3}.

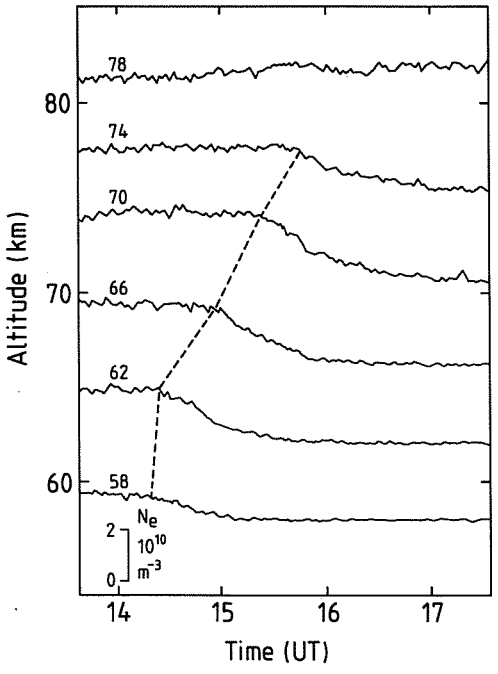

Figure 8*b*

Time series of electron density at selected heights during the sunset period on 23 *October, indicating the quality of the results from which the contours in Figure* 8*a were constructed (*2-min *averages). The label for each curve signifies the altitude from which the measurements are taken and the zero level for each curve is at the position corresponding to the altitude gate on the altitude axis. The broken line joins times when the electron density started to decrease from steady daytime values at each height.*

The final operation of GEN-11 during PCA conditions was for a 2-hour period just before local noon on 1 December, when the solar zenith angle was close to 92°. Densities derived from the radar measurements showed little variation with time. Figure 9 illustrates a typical profile from this period, which was at the peak of the SPE with fluxes close to 7000 pfu (> 10 MeV).

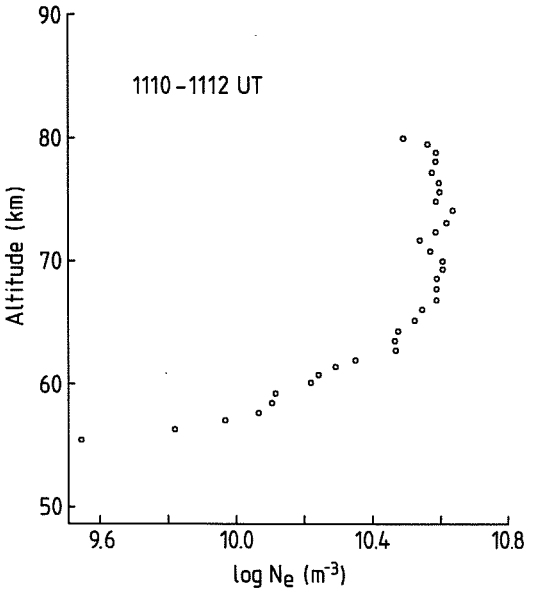

Figure 9

Electron density profile from the operation of GEN-11 *near local noon on* 1 *December,* 1989.

This SPE also included particles with energies greater than 100 MeV. Densities above 65 km were very similar to those observed on 20 and 23 October (Figs. 6 and 7) but showed a steeper decrease than the former two below 65 km. This could be explained by differences in the proton flux characteristics. However, changes in negative ion chemistry are important at twilight and results from other days (presented later) predict that, in comparison with daytime conditions, the electron density will show a decrease below 65 km altitude for a solar zenith angle of 92°, exactly as observed in this example (see section on twilight effects).

Power profile results (CP-1 and CP-2)

Three EISCAT operations during SPE's in 1989 fall into this category. The longest sequence of observations during strong PCA conditions was obtained by experiment CP-2, which was started at the end of the GEN-11 run on 23 October and continued for almost two days. The two other data sets of CP-1 type results were the evening before, and immediately after, the GEN-11 run of 1 December.

The most useful results from the CP-2 experiment for the present purpose are the power profile measurements, yielding electron densities down to 59 km from the lowest antenna elevation. Proton fluxes during this experiment were moderately large, with a significant enhancement late on 24 October (Fig. 5). An overview of the time variations of electron density is given in Figure 10, which shows results from four altitudes below 69 km as well as from four others between 69 and 85 km. Also included in the figure are the variation of solar zenith angle through the experiment and measurements of radio absorption from two riometers at approximately the same geomagnetic latitude in Scandinavia as the EISCAT radar.

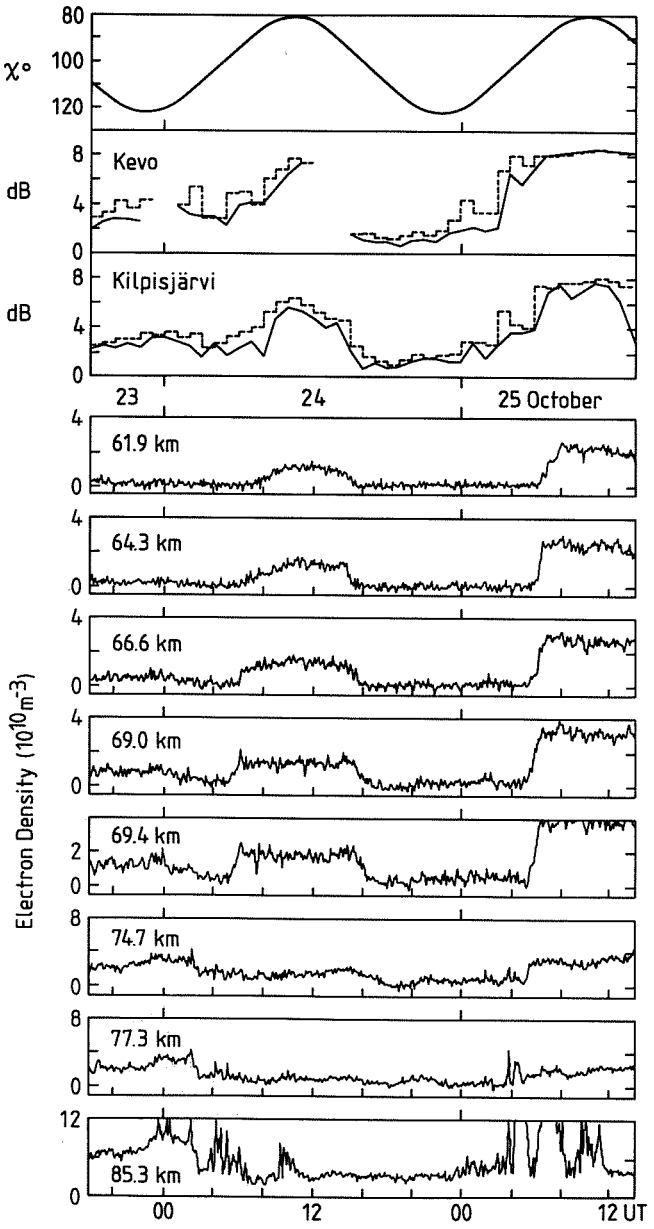

Figure 10

Time series of electron density from a range of altitudes between 62 *and* 85 km *measured by experiment* CP-2, 23-25 *October*, 1989. *Also shown are the solar zenith angle* (χ) *and radio absorption* (dB) *at about the same magnetic latitude as EISCAT in northern Scandinavia, measured by riometers at Kevo* ($L = 6.0$) *and Kilpisjärvi* ($L = 5.9$). *Full lines indicate the absorption measured during the first minute of each hour and broken lines the maximum absorption in each hour. Data gaps are due to interference.*

Two distinctive features can be noticed in the EISCAT observations in Figure 10. First, a diurnal modulation in the densities at the lower heights (below about 75 km), and second, more irregular features in time above about 75 km. As before, these two phenomena can be attributed to precipitation of protons and electrons, respectively. Note that there is no obvious immediate response in the ionosphere to the proton flux increase near 18 UT on 24 October. Rather, the increase appeared at sunrise on the next day when the densities below 70 km became twice as large as on the previous day. Density profiles from near local noon on 24 and 25 October are illustrated in Figure 11, emphasing the greater degree of ionisation at the lower altitudes on the 25th, but at these times the densities above 80 km were larger on the 24th.

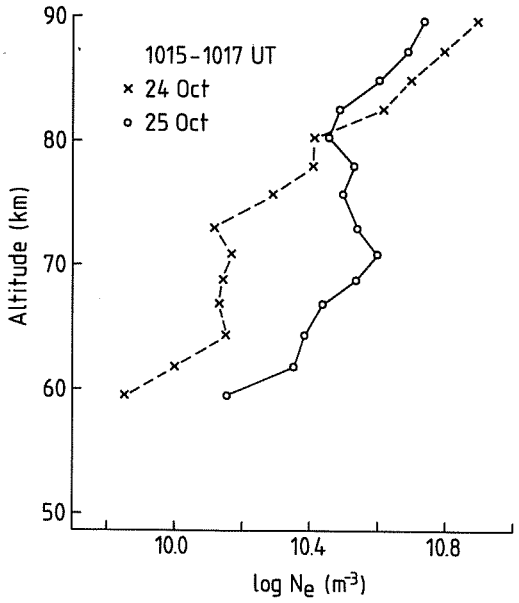

Figure 11

Daytime profiles of D-region electron density from experiment CP-2 *on* 24 *and* 25 *October*, 1989.

Finally, we present in Figure 12 two profiles from the evenings of 30 November and 1 December, which represent the onset and the declining phase, respectively, of the SPE whose main phase was captured by the GEN-11 observations on 1 December discussed above. The profile shapes are quite similar to each other, though different in magnitude. Much larger densities were observed below 80 km during the peak of the event, however (Fig. 9), though that was under twilight conditions while the two examples in Figure 12 are during the night. Although from different

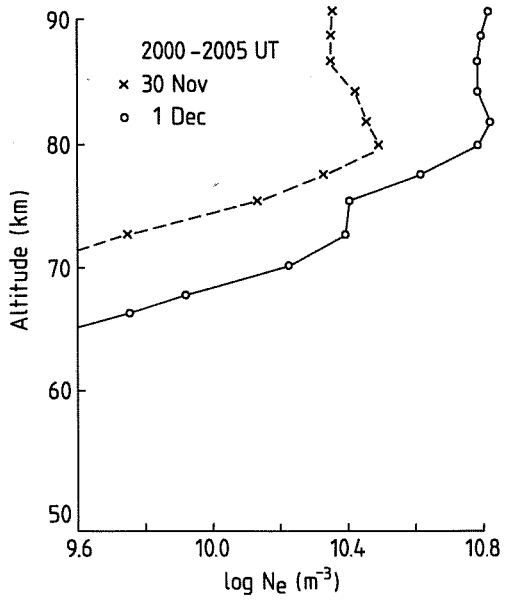

Figure 12
Nighttime profiles of D-region electron density from the evenings of 30 November and 1 December, 1989.

events, a comparison of Figures 11 and 12 immediately shows the reason for the difference in radio absorption between day and night during PCA's : there is a steep gradient of electron density just below 80 km at night. As will be discussed later, the « missing » electrons during the night at these lower heights are lost through attachment, forming negative ions which do not contribute to radio absorption.

5. RELATIONSHIP BETWEEN PROTON FLUX AND *D*-REGION ELECTRON DENSITY

Proton fluxes at geostationary orbit are constantly monitored with real-time availability. For the lowest part of the *D*-region not affected by electron precipitation, it should be possible to use the observed proton fluxes during PCA's as a predictor of mesospheric electron densities. This approach is analogous to, but simpler than, the method relating energetic electron observations at geostationary orbit with *D*-region densities during auroral radio absorption events (Collis *et al.*, 1984), since the latter was based on the magnitude of radio absorption but in the present case we have direct measurements of electron concentration.

To avoid difficulties associated with twilight changes in electron density (see later), periods of comparison of EISCAT and satellite data were restricted to when the solar zenith angle was smaller than 89° (day) or larger than 98° (night). This meant exclusion of the polar night operations in November and December (Table 2) from the daytime category. The March data were not used because EISCAT did not measure below 70 km altitude and the April experiment was excluded because of the complex variations in proton flux (Fig. 1). Nighttime densities were very small below 70 km (e.g. Fig. 12) so the analysis was confined to sunlit periods. Table 3 lists the dates and times of

Table 3
EISCAT/proton flux comparison. Proton fluxes are taken from Solar Geophysical Data (1989). *Fluxes* > 10 MeV *have been reduced by a factor of* 0.55 *(see text). « Figure » refers to the figure number in the text where the electron density results are displayed.*

Date (1989)	(UT)	Figure	Flux > E MeV (cm^2 s sr)$^{-1}$ E = 10	E = 30	E = 100
20 Oct	1144	6	2200	1000	115
23 Oct	1300	7	2750	1250	60
24 Oct	1015	11	550	200	9
25 Oct	1015	11	1650	600	50

the comparisons. This Table also contains the flux values above three threshold energies taken from Solar Geophysical Data (1989). As noted earlier, the published values for the lowest energy threshold have been corrected for their original overestimation.

Figure 13 displays the relationship of the proton fluxes with electron densities from heights of 70, 65,

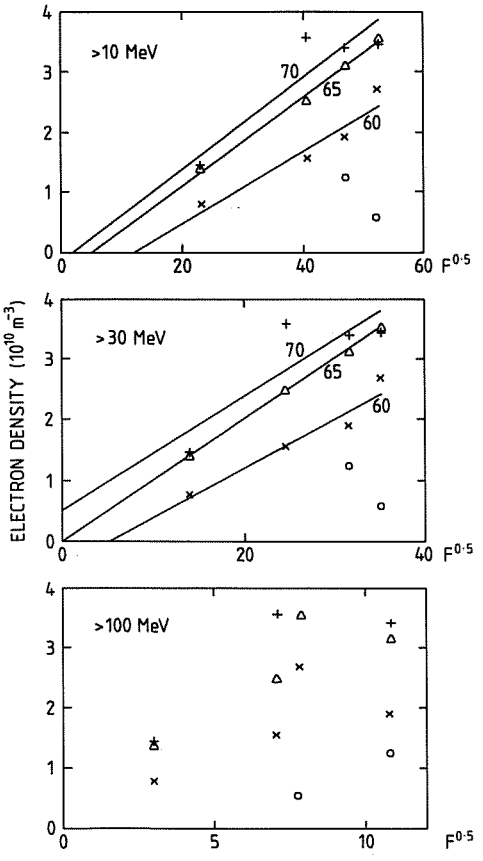

Figure 13
Electron density at selected altitudes as a function of the square root of the integral proton flux (F pfu*) above three threshold energies observed simultaneously at geostationary orbit. Proton fluxes are taken from Solar Geophysical Data* (1989). *The* < 10 MeV *values have been reduced by a factor of* 0.55 *from the published values as discussed in the text. Linear fits to the points for* 60, 65 *and* 70 km *altitude are labelled as* 60, 65 *and* 70, *respectively. The symbols indicate the different heights of the electron density measurements :* 55 km (O), 60 km (×), 65 km (△) and 70 km (+).

60 and, where available, 55 km altitude. The square root of the particle flux is used in the figure because electron density should be proportional to the square root of the ion production rate, and hence to the square root of the proton flux. For nighttime, we observed the result that proton fluxes of these energies cannot be used to predict electron densities between 60 and 70 km altitude. This arises because most of the negative charge at these heights at night resides in negative ions and nighttime radio absorption during PCA's responds mainly to fluxes of a few MeV (see below).

The daytime results in Figure 13 show much more promise than the nighttime periods for reliable prediction of mesospheric electron concentrations. Fluxes > 10 MeV and > 30 MeV show approximately equally good linear relationships with densities at 60 and 65 km with most scatter at 70 km (Table 4). The > 100 MeV results have poorer correlation, but are the only one of the three sets to show larger fluxes with larger density at 55 km (albeit with only two data points). However, since in general some events do not include fluxes > 100 MeV we do not consider these further for predictive purposes.

Table 4 displays the coefficients of the linear fits to the points for fluxes > 10 MeV and > 30 MeV for heights of 60, 65 and 70 km. These fits are also included in Figure 13, and indicate by their intercepts on the two abscissae that significant densities are expected at 60 km only when fluxes exceed some threshold (about 100 pfu > 10 MeV and 25 pfu > 30 MeV). Two points should be remembered if these results are to be used for ionospheric predictions. First, the statistical significance is limited since we only include four intervals, but for all the cases in Table 4 the standard error in the derived slopes is smaller than 10 %. For the two examples with $r = 0.99$ the error is smaller than 5 %. It would obviously be desirable to assemble a larger set of data. Secondly, the results are from a limited time interval and seasonal differences may exist in reality (related to changes in the neutral atmosphere).

Table 4

Predictions of electron density at 60, 65 *and* 70 km *altitude from integral proton fluxes* > 10 MeV *and* > 30 MeV. *The coefficients indicate the multiplicative factor* (B) *needed to obtain the electron density at the given height from the square root of the integral flux* F $(\mathrm{cm}^2\ \mathrm{s\ sr})^{-1}$ *above the stated threshold energies, to which the intercept* (A) *should be added, according to* $N_e = A + BF^{0.5}$, *in units* $10^{10}\ \mathrm{m}^{-3}$. *The correlation coefficients of the fits are given by the quantity* r.

Altitude (km)	Integral proton flux threshold energy > 10 MeV			> 30 MeV		
	A	B	r	A	B	r
60	−0.74	0.06	0.96	−0.42	0.08	0.96
65	−0.37	0.07	0.99	−0.42	0.08	0.99
70	−0.13	0.08	0.91	+0.55	0.09	0.84

6. TWILIGHT EFFECTS

The day/night differences in D-region electron density during SPE's were already recognised in the earliest absorption measurements (Bailey, 1957). Since the particle flux does not usually change much through the sunrise and sunset periods (i.e. the ion-production rate is almost constant), the changes in electron density must be due to increased loss in the absence of sunlight, with the implication of changes in neutral and/or ion constituents at the heights affected. Much attention has focused on the influence of negative ions in this process, in particular the role of atomic oxygen (Adams and Megill, 1967; Reid, 1969). Detailed studies of twilight variations in radio absorption during PCA's have been important in investigating the effects governing changes in electron density (Chivers and Hargreaves, 1965).

EISCAT's observations during the second half of October, 1989, provided continuous measurements of D-region densities for 50 h, covering four successive twilight periods (Figs. 8 and 10). Proton fluxes were large throughout this interval (Fig. 5), ensuring good accuracy in the radar measurements. An inspection of Figures 8 and 10 reveals that the times of twilight changes in electron density have an altitude dependence. More accurate examination of the time series of electron density at particular heights allows the time of the initial twilight deviation (increase at sunrise; decrease at sunset) to be determined. The best height- and time-resolution observations for this interval are those from GEN-11, covering the first sunset period (23 October). Figure 14 (upper panel)

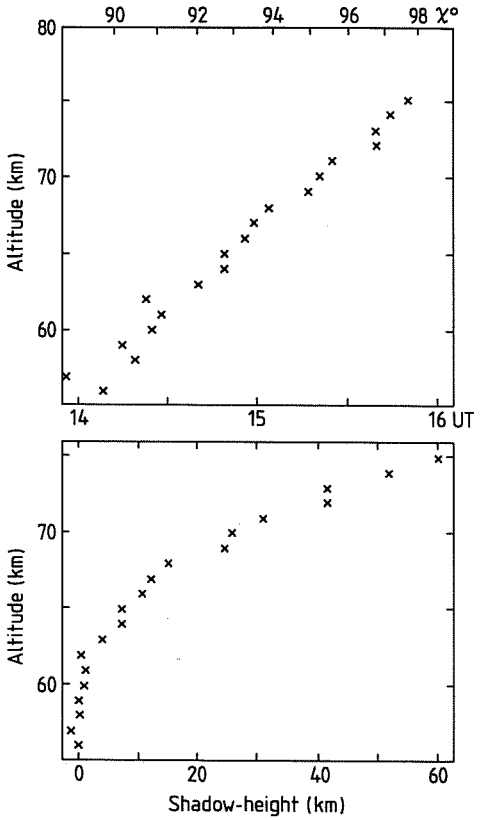

Figure 14

Top: height of initial decrease of electron density during the sunset period on 23 *October,* 1989, *as a function of* UT. *Solar zenith angle* (χ) *is also shown.*
Bottom: as above but with earth's shadow-height as the abscissa.

shows the heights of first decrease of electron density as a function of time (indicated also by the broken line in Fig. 8b for some altitudes). The dependence is essentially linear with time (or, equivalently, with solar zenith angle, which is also included in Fig. 14). At 55 km, the lowest altitude measured, the depletion started already at a solar zenith angle close to 90° i.e. ground sunset, when the lower mesosphere was still receiving visible sunlight. The points in the upper panel of Figure 14 are replotted in the lower panel, where the abscissa is now the height of the shadow of the solid earth in the atmosphere. This emphasises that at all heights the mesosphere was still sunlit when the density depletions commenced, though there is a clear breakpoint at about 67 km, where the rate of change of depletion-height with shadow-height abruptly decreases.

Moving now to a sunrise period, we chose data from the morning of 25 October (when densities were larger than on 24 October) for comparison with the results in Figure 14. Figure 15 (upper panel) illustrates time series of electron density measured by the CP-2 experiment from selected altitudes during the sunrise period. From this interval we estimated the times when the first indication of an increase of electron density from steady nighttime values was apparent at a given altitude; these estimates are joined by the broken lines in Figure 15. The scanning motion of the antenna imposes an uncertainty of up to 6 min in this estimation. The times of the increases are shown in Figure 16, which has the same format as Figure 14, though of course the sense of change in the upper panels is opposite for the two cases. When comparing the results in Figures 14 and 16, we should remember that the observations from 25 October have coarser height-resolution than those from 23 October, but a larger number of different heights were sampled due to the antenna scanning motion. A more complicated variation of twilight effect with time is evident at sunrise, in contrast to the linear variation at sunset. Two height regimes can be identified in the sunrise

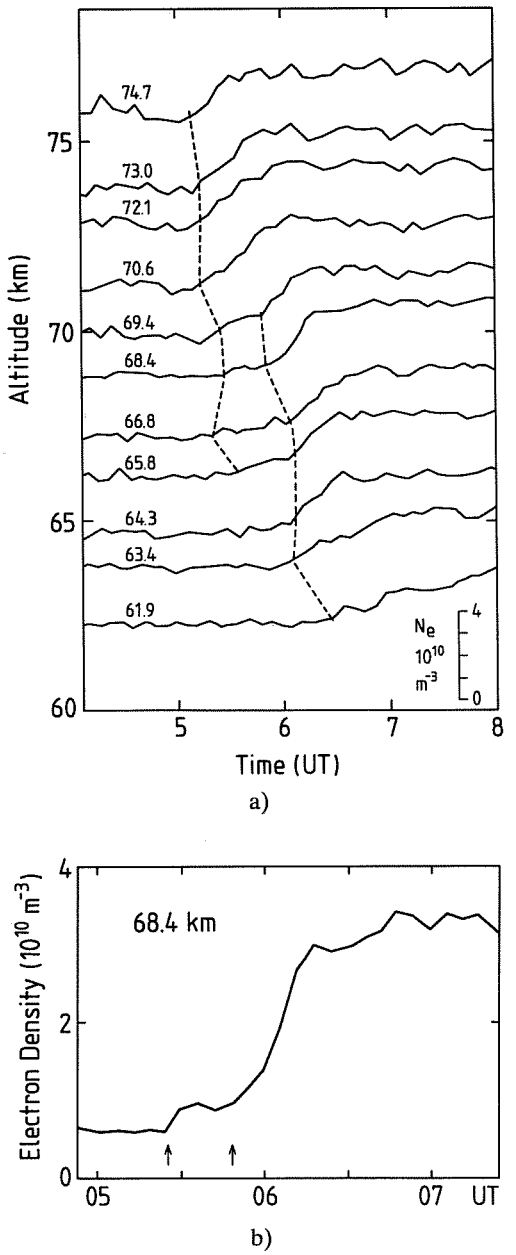

Figure 15

Upper panel: examples of time series of electron density at selected heights from experiment CP-2 *during the sunrise period on* 25 *October,* 1989. *Each point is a* 90-s *average every* 6 min; *uncertainties vary with signal strength but are of the order of* 10 % *(the size of the arrows in the lower panel). Broken lines join the estimated times of initial increase of electron density above the nighttime values (shown in more detail in Figure* 16*). The label for each curve signifies the altitude from which the measurements are taken and the zero level for each curve is at the position corresponding to the altitude gate on the altitude axis. Lower panel: example of the two-step increase of electron density in the overlap region at* 68.4 km. *Arrows mark the times of the two separate increases.*

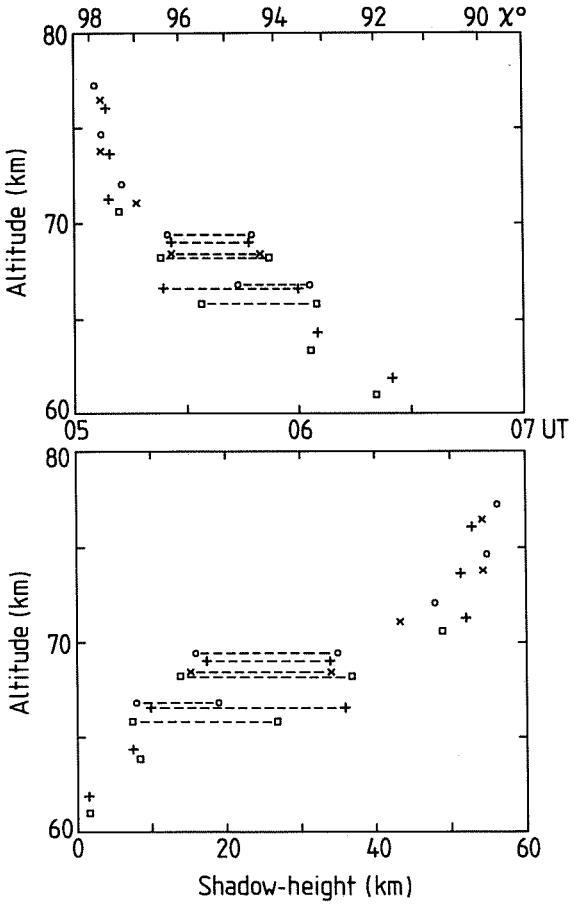

Figure 16

As Figure 14, *but for density increases during the sunrise period on* 25 *October. Horizontal broken lines indicate where two increases of electron density were observed (see text). The symbols indicate which antenna positions the points correspond to:* 89.9° (×), 77.5° (○), 62.6° (□) *or* 60.4° (+).

results, with a region of overlap between about 66 and 70 km altitude. In fact, the time series of electron density from all altitude gates in this overlap region were found to include *two* increases, the earlier of which fitted with the trend of higher altitudes, and the later with lower altitudes. Figure 15 includes four examples of this phenomenon. The lower panel of Figure 15 is an expanded version of the measurements from 68.4 km altitude: the density first increased above the constant nighttime value between 0524 and 0530 UT. It then remained at this new value for four 6-min scans of the experiment, before increasing more rapidly to the steady daytime value over the next hour. When plotted against shadow-height, the two altitude regimes show almost the same linear slopes, but with an offset of about 20 km in shadow-height in the overlap region (Fig. 16, lower panel). This slope is similar to that below the breakpoint in the lower panel of Figure 14.

Density variations during sunrise and sunset on 24 October were not so clearly determined as the above two cases. In part, this was due to generally lower densities (and associated higher noise levels) making it more difficult to define precisely when the twilight change commenced, but also, for sunrise particularly, the increase was much less sharp on 24 October and was not seen at such high altitudes (only below 74 km), compared with 25 October (see Fig. 10). However, without showing the data here, we state that the results are fully consistent with those in Figures 14 and 16, with the exception that the double increase at sunrise (Fig. 15) could not be identified above the noise level of the measurements on 24 October.

All the above observations of variations during twilight suggest that there is a fundamental difference in *D*-region chemistry below about 66 km altitude and above about 70 km during the PCA conditions reported here. Heights between 66 and 70 km represent a transition between the two regimes. We now summarise these properties, with particular reference to Figures 14 and 16.

At sunrise, the electron densities at heights between 77 and 70 km altitude successively increase as the earth's shadow moves down from 55 to 45 km altitude (solar zenith angle changing from 97.5° to 96.5°). The additional 20-25 km « shadow » corresponds to the height of the ozone layer, which absorbs solar ultraviolet (UV) radiation. Hence it is UV, rather than visible light, which is responsible for detaching the electrons from pre-existing negative ions at this time, implying that the negative ion in question is not O_2^- (which has a small electron affinity and is easily photodetached by visible light). Although O_2^- should be the principal initial ion in mesospheric ion chemical schemes, being produced by three-body attachment on oxygen molecules, it is expected that further reactions, *via* O_3^- and O_4^- with CO_2 or NO, will produce « terminal » ions of the types HCO_3^-, CO_3^-, CO_4^-, NO_2^- or NO_3^-, some of which may also be hydrated (Ferguson, 1974; Reid, 1976; Thomas, 1983). Our results indicate that the ions present have relatively high electron affinity and require photons of UV energy to detach the electrons. This result agrees with the discrepancy found by Reid (1961) when comparing twilight variations of PCA observed by riometer and calculated assuming O_2^- was the sole negative ion. The existence of all the above ions in the mesosphere has been inferred from rocket-borne experiments, though a likely candidate for the high affinity ion is NO_3^-, since CO_3^- is easily photodissociated by visible sunlight (Peterson, 1976). By studying the onset times of strong echoes at 72 km altitude measured by the Poker Flat 50 MHz MST radar at sunrise, Reid (1987) showed that photodissociation of the nighttime negative ions corresponded with UV, rather than visible sunrise. It was concluded that NO_3^- generally dominated over CO_3^- due to the variable, but often relatively large, concentrations of NO in the auroral-zone mesosphere. Further information is badly needed to improve knowledge of mesospheric negative ion chemistry.

Our observations show that release of electrons by UV photodetachment decreases in importance below 70 km and appears to be inoperative below 66 km. The initial increase at e.g. 68.4 km in Figure 15 is the remaining signature of this process, while the second, larger increase in that figure represents an additional source of electrons. Production of this second source of electrons is delayed by about 30 min after the UV has penetrated a given altitude: at these times the solid earth's shadow is about 50 km below the altitude where the electron density begins to increase. The highest altitude at which this delayed effect is observed is about 70 km, it then becomes progressively more important down to 65 km, at which height it is totally dominant. Since there is a considerable delay in the production of the electrons following illumination by UV, it is difficult to interpret this second source as simple photodetachment if UV is involved. More likely, we feel, the delay of 30 min or so is a characteristic time for the build-up of atomic oxygen and $O_2(^1\Delta_g)$ during the sunrise period at these heights (Swider, 1977). Atomic oxygen reacts with molecular oxygen to produce ozone, and ozone itself is photodissociated by UV back to molecular oxygen in both its ground state and first excited state ($^1\Delta_g$). Suggestions that collisional detachment of $O_2(^1\Delta_g)$ with O_2^- ions might be important during PCA events were presented by Megill and Hasted (1965). This reaction was included in the scheme of Adams and Megill (1967) who showed model profiles of $O_2(^1\Delta_g)$ during twilight conditions and calculated that collisional detachment with O_2^- would be the major loss process for this ion below 68 km during twilight.

Although we suggested above that most of the O_2^- ions which are produced in the mesosphere are converted to terminal ions, this may not always be the case for all conditions. Mitra (1975), for example, applied a six-ion model of mesospheric chemistry, in which all negative ions other than O_2^- were treated as a single species, in a study of a range of disturbed ionospheric conditions. For PCA events he found that the proportion of simple ions relative to terminal-type ones was larger than that expected during undisturbed conditions, for both day and night. Although this

result applied only above about 68 km (the range 55-85 km was presented), it could be expected that fine-tuning of the model might move this region to lower altitudes. However, the rocket observations of Viggiano *et al.* (1982) showed that, at least under the weakly disturbed auroral conditions of their experiment, O_2^- was not a major ion at altitudes below 83 km. If this also turns out to be true for PCA conditions, then an alternative explanation of the delayed increase of electron density below 70 km at sunrise is needed since the mechanism of Adams and Megill (1967) described above requires O_2^-.

We can still attribute the delay to the time required for neutral oxygen species to build up at sunrise, but consider instead the atomic oxygen itself, rather than the secondary product $O_2(^1\Delta_g)$. Although the ions O_3^- and CO_3^- can be photodissociated by visible sunlight, and the product O^- then photodetached (Peterson, 1976), these two ions also undergo reactions with atomic oxygen to produce O_2^- (e.g. Ferguson, 1974), which is also easily photodetached. Hence if atomic oxygen controls the fate of O_3^- and/or CO_3^-, then release of free electrons at sunrise will follow the growth of the atomic oxygen concentration. A quantitative analysis of this scheme is beyond the scope of this paper, but it is clear that additional modelling work is required to understand the observations.

At sunset (Fig. 14), decreases in electron density were seen initially near 55 km altitude ($\chi = 89°$) and successively over the next half hour up to 62 km ($\chi = 91°$). Throughout this time the earth's shadow was still within about 1 km of the earth's surface. This initial commencement near $\chi = 89°$ is as observed during the twilight depletion of radio absorption during PCA events (Chivers and Hargreaves, 1965) and consistent with the predictions of the Adams and Megill (1967) model. Subsequent depletions towards higher altitudes represent an inverse of the sunrise increases, with the exception that at sunset there is no direct correspondence to the time delay for build-up of neutral oxygen species in the 66 to 70 km region. Rather, the times of the electron density decreases at heights up to about 68 km are functions of the twilight-decay behaviour of the O or $O_2(^1\Delta_g)$ profiles, though it is outside the scope of the present study to analyse these in detail. Above 68 km, the times of initial electron density decrease are again in the region where the mesosphere is rapidly falling into the shadow of the earth's UV layer, allowing attachment of the electrons to neutrals. In this region, the lifetime of atomic oxygen becomes much longer than for lower altitudes (Adams and Megill, 1967). Since the neutral atmosphere plays an important role in determining the equilibrium electron density, it is possible that the precise height dependence seen in Figures 14 and 16 may show some seasonal variation according to changes in the density of the neutral atmosphere. Further observations during other seasons are needed to investigate this possibility.

It is not immediately clear why the relationship between depletion-altitude and solar zenith angle at sunset (Fig. 14) is linear. As noted above, the results from the next sunset period (24 October, not shown here) were very similar, both yielding values of 2.1 km per degree. It will be instructive to obtain further data to see whether this dependence changes for other times of year when the solar zenith angle changes at a different rate.

7. NIGHTTIME λ PROFILES

A further day/night comparison is shown in Figure 17. Here we display as broken lines the arithmetic differences between the nighttime and daytime electron density profiles for sunset on 23 October (+ symbols) and sunrise on 25 October (O symbols). These differences are normalised to the relevant nighttime profile. For sunrise, the two profiles are from 04 and 08 UT (solar zenith angles of 103° and 85°, respectively) and for sunset, from 14 and 18 UT (solar zenith angles 81° and 101°, respectively). The broken line results in Figure 17 would represent profiles of λ, the classical ratio of negative ion number density to electron number density, if there were no negative ions present by day and if all the « missing » electrons formed negative ions at night. Theoretical and observational work suggest a steady increase of λ with decreasing altitude, though the absolute magnitude of this quanti-

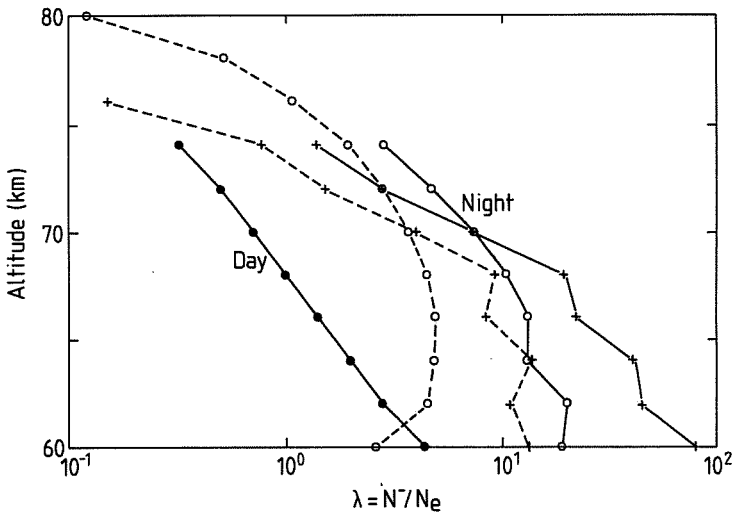

Figure 17
Broken lines : profiles of differences between daytime and nighttime electron density, normalised to the nighttime values, for the periods before and after sunset on 23 October (+) and before and after sunrise on 25 October (O). Full circles (day) : assumed daytime profile of λ (from Ulwick, 1973). Full lines (night) : deduced nighttime profiles of λ for 23 (+) and 25 (O) October.

ty is relatively uncertain, depending upon, e.g. geophysical conditions (Mitra, 1981). The non-monotonic increase of the broken lines with decreasing height in the results in Figure 17 implies that significant concentrations of negative ions are indeed present below 66 km by day. As a model for the λ profile during daytime, we take a mean of the values derived by Ulwick (1973) from rocket measurements during the PCA of 2/3 November 1969, indicated by the full circles in Figure 17. As stated by Ulwick (1973), λ during daytime is a characteristic parameter of the atmosphere and should not be very sensitive to changes in production rate and electron density. We can then calculate the number density of negative ions during the nighttime periods of the two twilight intervals by assuming that the number of negative ions present by day (λN_e) are also present at night, and that the difference in magnitude of nighttime and daytime electron densities is due to the « missing » daytime electrons having attached to neutral atoms or molecules to form negative ions. The results of this analysis are displayed as the full lines labelled « Night » in Figure 17. Reasonable agreement is obtained between the two nighttime profiles, though their accuracy is limited by how well the nighttime electron densities are measured.

8. DISCUSSION AND CONCLUSIONS

a) Spatial variation of electron density during PCA's

It is commonly assumed that the proton precipitation during PCA's is spatially uniform within the affected polar cap area. Our measurements show no evidence to contradict this, provided that the fine structure in the time variations of electron density at heights of 75-80 km and above is due to energetic electron precipitation. Studies aimed at determining recombination coefficients from observations of ionospheric electron density and precipitating charged particle fluxes during SPE's should therefore always consider the effects of electron precipitation in order to avoid possible erroneous interpretation. It becomes even more difficult to apply this approach if the ionospheric observations are near the edge of the proton precipitation area. A geostationary satellite will detect proton fluxes of all energies, but the geomagnetic field acts as a filter, preventing particles below a particular energy from penetrating equatorward of the so-called cut-off latitude, as predicted in principle by Störmer theory. The difference between the true geomagnetic field and a dipole field allows protons to reach further equatorward, but imposes a sharper boundary, than predicted by Störmer theory (Reid and Sauer, 1967). By defining the edge of the PCA region to lie between the cut-offs of 1 and 100 MeV protons, Reid (1970) suggested that this would cover about 500 km in the ionosphere. Allen *et al.* (1989) show geomagnetic cut-offs from polar-orbit satellite measurements for the 13 March, 1989 event. A sufficiently dense latitudinal chain of riometers could delineate this boundary, but information on the distribution of electron density, in height and latitude, can only be determined from measurements such as those from CP-3 (Figs. 2 and 3).

b) Vertical profiles of electron density during PCA's

The exact shape of the electron density profile during PCA's depends on the flux and energy spectrum of the precipitating protons under sunlit conditions. At night, the much higher electron loss rates at the lower altitudes severely modify the shape of the profile, giving rise to the characteristic diurnal variation of electron density (Fig. 10) and of radio absorption, which is typically a factor of 3 to 7 smaller at night (Gillmor, 1963). Our results show that this effect becomes increasingly important at altitudes below 75 km (compare e.g. Figs. 11 and 12), being related to the diurnal variations in atomic oxygen or electronically excited molecular oxygen. These figures can be compared with the results of Reid (1969), who showed that nighttime radio absorption during PCA's was best correlated with proton fluxes of energy 3 to 10 MeV (a 5 MeV proton penetrates to 73 km altitude) while daytime absorption was due mainly to fluxes of the order of 20 MeV (penetrating to 54 km) and higher. Hence we were able to deduce meaningful empirical relationships between electron density at heights between 60 and 70 km and integral proton fluxes > 10 and > 30 MeV for daytime, but not for nighttime.

c) Twilight chemistry

Detailed study of the time variations during sunrise and sunset have shown the controlling influence of changes in neutral oxygen chemistry in the build-up and decay of electron concentration. In particular, the so-called « twilight anomaly » observed in riometer measurements, representing the relatively smaller absorption at sunrise compared with sunset for the same solar zenith angle, is explained by the time taken for the build-up of atomic oxygen or metastable oxygen molecules at heights below about 70 km. This effect would also be expected to introduce corresponding time variations in the transition of the λ profile from its steady daytime to nighttime values. Our observations agree closely with the predictions of the model of Adams and Megill (1967), whereby O_2^- ions are converted to a more stable species governed by ultraviolet photochemistry (possibly NO_3^-). In this model, the loss of O_2^- below about 70 km during sunrise depends mainly on collisional detachment with $O_2(^1\Delta_g)$. If O_2^- is not a major ion at these heights, the delayed increase in release of free electrons may depend on the time variations of atomic oxygen itself, through reactions with other species such as O_3^- or CO_3^-. Further experimental data and combined studies using ion chemical models are essential to investigate the relative importance of these processes.

d) Final remarks

Table 2 indicates that a substantial data base of EISCAT observations during PCA conditions was accumulated during 1989. In part, this was due to the relatively large number of events, but it was also due to having ready-prepared experiments available for such conditions, and the ability to call on radar and

staff resources at short notice during periods when normally no operations were scheduled. This state of readiness should obviously be maintained over the next 2-3 years, by which time a significant amount of new information should have been collected before the frequency of PCA events starts to diminish as the next solar minimum approaches.

Particular goals for further observations should include the following :

i) Operation of a special-purpose low-altitude experiment (such as GEN-11) for a longer interval, to allow good definition of longer period dynamical processes such as the semi-diurnal tide (Rietveld and Collis, 1990), and to include better height-resolution measurements for a sunrise period than those from CP-2 in October 1989. In practice, the latter condition means starting operations on the preceding day. None of the GEN-11 operations in Table 2 was longer than 9 h.

ii) Acquisition of similar high-resolution low-altitude data with the VHF radar. In principle, the VHF system should be even more suitable for such studies than the UHF one.

iii) Simultaneous operation of low-altitude experiments on the UHF and VHF radars together. This would be of particular interest for detailed comparison of the spectral measurements and for better appraisal of the technique in general.

iv) Dual experiment studies with the VHF radar making mesospheric observations and the UHF making more general-purpose thermosphere/ionosphere measurements. Such data would be important for studies of coupling between the mesosphere and higher altitudes.

Acknowledgements

The EISCAT Scientific Association is supported by the Centre National de la Recherche Scientifique of France, Suomen Akatemia of Finland, Max Planck Gesellschaft of West Germany, Norges Almenvitenskaplige Forskningsråd of Norway, Naturvetenskapliga Forskningsrådet of Sweden and the Science and Engineering Research Council of the United Kingdom. We appreciate the prompt supply of riometer data from Sodankylä Geophysical Observatory (H. Ranta) and liaison with the Space Environment Services Division of NOAA (J. A. Joselyn and J. M. Kunches).

REFERENCES

Adams, G. W., and L. R. Megill, A two-ion *D*-region model for polar cap absorption events, *Planet. Space Sci.*, **15,** 1111-1130, 1967.

Allen, J., L. Frank, H. Sauer, and P. Reiff, Effects of the March 1989 solar activity, *Eos,* 1479-1488, 1989.

Arnold, F., A. A. Viggiano, and E. E. Ferguson, Combined mass spectrometric composition measurements of positive and negative ions in the lower ionosphere, II. Negative ions, *Planet. Space Sci.*, **30,** 1307-1314, 1982.

Bailey, D. K., Disturbances in the lower ionosphere observed at VHF following the solar flare of 23 February, 1956 with particular reference to auroral zone absorption, *J. Geophys. Res.*, **62,** 431-463, 1957.

Bailey, D. K., Abnormal ionisation in the lower ionosphere associated with cosmic-ray flux enhancements, *Proc. I.R.E.*, **47,** 255-266, 1959.

Bailey, D. K., Polar cap absorption, *Planet. Space Sci.*, **12,** 495-541, 1964.

Baron, M., The EISCAT facility, *J. Atmos. Terr. Phys.*, **46,** 469-472, 1984.

Chivers, H. J. A., and J. K. Hargreaves, Conjugate observations of solar proton events : delayed ionospheric changes during twilight, *Planet. Space Sci.*, **13,** 583-592, 1965.

Collis, P. N., and I. Häggström, Plasma convection and auroral precipitation processes associated with the main ionospheric trough at high latitudes, *J. Atmos. Terr. Phys.*, **50,** 389-404, 1988.

Collis, P. N., and J. Röttger, Mesospheric studies using the EISCAT UHF and VHF radars : a review of principles and experimental results, *J. Atmos. Terr. Phys.*, **52,** 569-584, 1990.

Collis, P. N., J. K. Hargreaves, and A. Korth, Auroral radio absorption as an indicator of magnetospheric electrons and of conditions in the disturbed auroral *D*-region, *J. Atmos. Terr. Phys.*, **46,** 21-38, 1984.

Eriksen, K. W., O. Holt, and B. Landmark, A note on the polar absorption event of 11-18 May, 1959, *J. Atmos. Terr. Phys.*, **18,** 78-81, 1960.

Ferguson, E. E., Laboratory measurements of ionospheric ion-molecule reaction rates, *Rev. Geophys. Space Phys.*, **12,** 703-713, 1974.

Folkestad, K., T. Hagfors, and S. Westerlund, EISCAT : an updated description of technical characteristics and operational capabilities, *Radio Sci.*, **18,** 867-879, 1983.

Gillmor, C. S., The day-to-night ratio of cosmic noise absorption during polar cap absorption events, *J. Atmos. Terr. Phys.*, **25,** 263-266, 1963.

Hakura, Y., Solar cycle variation in particle emissivity of the sun, *Solar Phys.*, **39,** 493-497, 1974.

Hargreaves, J. K., H. Ranta, A. Ranta, E. Turunen, and T. Turunen, Observations of the polar cap absorption event of February 1984 by the EISCAT incoherent scatter radar, *Planet. Space Sci.*, **35,** 947-958, 1987.

Little, C. G., and H. Leinbach, The riometer — a device for the continuous observation of ionospheric absorption, *Proc. I.R.E.*, **47,** 315-320, 1959.

Megill, L. R., and J. B. Hasted, Free electron balance during polar cap absorption events, *Planet. Space Sci.*, **13,** 339-343, 1965.

Mitra, A. P., *D*-region in disturbed conditions, including flares and energetic particles, *J. Atmos. Terr. Phys.*, **37,** 895-913, 1975.

Mitra, A. P., Chemistry of middle atmosphere ionisation : a review, *J. Atmos. Terr. Phys.*, **43,** 737-752, 1981.

Narcisi, R. S., A. D. Bailey, L. Della Luca, C. Sherman, and D. M. Thomas, Mass spectrometric measurements of negative ions in the *D*- and lower *E*-regions, *J. Atmos. Terr. Phys.*, **33,** 1147-1159, 1971.

Peterson, J. R., Sunlight photodestruction of CO_3^-, CO_3^- H_2O, and O_3^- : the importance of photodissociation to the *D* region electron densities at sunrise, *J. Geophys. Res.*, **81,** 1433-1435, 1976.

Reagan, J. B., and T. M. Watt, Simultaneous satellite and radar studies of the *D*-region ionosphere during the intense solar particle events of August 1972, *J. Geophys. Res.*, **81,** 4579-4596, 1976.

Reid, G. C., A study of the enhanced ionisation produced by solar protons during a polar cap absorption event, *J. Geophys. Res.*, **66,** 4071-4085, 1961.

Reid, G. C., Associative detachment in the mesosphere and the diurnal variation of polar-cap absorption, *Planet. Space Sci.*, **17,** 731-736, 1969.

Reid, G. C., Current problems in polar cap absorption, in: *Intercorrelated Satellite Observations Related to Solar Events,* D. Reidel Publ. Co., Dordrecht, Holland, 319-334, 1970.

Reid, G. C., Ion chemistry in the *D*-region, in: *Advances in Atomic and Molecular Physics,* **12,** Eds. D. R. Bates and B. Bederson, Academic Press, New York, 375-413, 1976.

Reid, G. C., Radar observations of negative-ion photodetachment at sunrise in the auroral-zone mesosphere, *Planet. Space Sci.*, **35,** 27-37, 1987.

Reid, G. C., and C. Collins, Observations of abnormal VHF radio wave absorption at medium and high latitudes, *J. Atmos. Terr. Phys.*, **14,** 68-81, 1959.

Reid, G. C., and H. H. Sauer, The influence of the geomagnetic tail on low-energy cosmic-ray cut-offs, *J. Geophys. Res.*, **72,** 197-208, 1967.

Rietveld, M. T., and P. N. Collis, Mesospheric observations with the EISCAT UHF radar during polar cap absorption events: 2. Spectral measurements, *Ann. Geophysicae,* to be submitted, 1990.

Rietveld, M. T., P. N. Collis, and J. Röttger, Observations of atmospheric dynamics in the low- and middle-mesosphere with the EISCAT incoherent scatter radar during solar proton events, *Adv. Space Res.*, in press, 1990.

Röttger, J., C. La Hoz, M. C. Kelley, U.-P. Hoppe, and C. Hall, The structure and dynamics of polar mesosphere summer echoes observed with the EISCAT 224 MHz radar, *Geophys. Res. Lett.*, **15,** 1353-1356, 1988.

Smart, D. F., and M. A. Shea, Solar proton event classification system, *Solar Phys.*, **16,** 484-487, 1971.

Solar Geophysical Data, 1989, issues according to dates of events, published by NOAA, Space Environment Services Center, 325 Broadway, R/E/SE2, Boulder, Colorado 80303, USA.

Svestka, Z., *Solar Flares,* D. Reidel Publ. Co., Dordrecht, Holland, 1976.

Swider, W., Aeronomic aspects of the polar *D*-region, *Space Sci. Rev.*, **20,** 69-114, 1977.

Thomas, L., Modelling of the ion composition of the middle atmosphere, *Ann. Geophysicae,* **1,** 61-73, 1983.

Turunen, T., GEN-system A new experimental philosophy for EISCAT radars, *J. Atmos. Terr. Phys.*, **48,** 777-785, 1986.

Turunen, E., H. Matveinen, H. Ranta, and P. Pollari, Day to night variations of *D*-region electron density observed by the EISCAT incoherent scatter radar during the PCA event on August 12-15, 1989, Paper presented at XV General Assembly of EGS, Copenhagen, 23-27 April, 1990.

Ulwick, J. C., Operation PCA69 — An investigation of the solar particle event of 2 November, 1969, *Space Res.*, **XI,** 1181-1187, 1971.

Ulwick, J. C., Steady state coefficients in the *D*-region during solar particle events, *Space Res.*, **XIII,** 581-586, 1973.

Viggiano, A. A., F. Arnold, D. W. Farley, F. C. Fehsenfeld, and E. E. Ferguson, Silicon negative ion chemistry in the atmosphere — *In situ* and laboratory measurements, *Planet. Space Sci.*, **30,** 499-506, 1982.

Zwickl, R., and J. M. Kunches, Energetic particle events observed by NOAA/GOES during solar cycle 22 (abstract), *Eos,* **70,** 1258, 1989.